International Journal of Mechanical, Industrial and Aerospace Sciences
ISSN: 2517-9950
Vol:13, No:2, 2019

Effectiveness Evaluation of a Machine Design Process Based on the Computation of the Specific Output

Barenten Suciu

***Abstract*—**In this paper, effectiveness of a machine design process is evaluated on the basis of the specific output calculus. Concretely, a screw-worm gear mechanical transmission is designed by using the classical and the 3D-CAD methods. Strength analysis and drawing of the designed parts is substantially aided by employing the SolidWorks software. Quality of the design process is assessed by manufacturing (printing) the parts, and by computing the efficiency, specific load, as well as the specific output (work) of the mechanical transmission. Influence of the stroke, travelling velocity and load on the mechanical output, is emphasized. Optimal design of the mechanical transmission becomes possible by the appropriate usage of the acquired results.

***Keywords*—**Mechanical transmission, design, screw, worm-gear, efficiency, specific output, 3D-printing.

I. Introduction

NOWADAYS, the optimal design of various machines is considered under two main conditions: to maximize the machine total efficiency, for energy saving and environmental protection, and to minimize the overall size, for compact and smart design [1]-[9]. However, in some cases, the influence of input design parameters on the machine efficiency cannot be clearly identified [10]-[14]. For example, in the case of screw-worm gear mechanical transmissions, especially for relatively large loading forces, the influence of some design parameters, such as the fixity coefficient [15] and/or the travelling velocity of the load [16] cannot be decisively emphasized.

For these reasons, in the present work a screw-worm gear mechanical transmission (SWGMT) is designed by the means of traditional [15], [17], and computer-aided design (3D-CAD) methods [18]. SolidWorks software [18] was preferred to assist the strength calculations and the drawing preparations. In order to check for the adequate fitting of the components, main parts are printed in ABS resin by using a 3D-printer. Effectiveness of the design process is evaluated by using both the classical total efficiency, and by defining the so-called specific output work of the machine. Purpose of this study is to decide without equivocation the optimal design conditions, based on the effect of input parameters on the specific output of the SWGMT.

II. Description of the Designed SWGMT

In addition to the brief description of the SWGMT given by [15], Fig. 1 illustrates the input (horizontal) wormed shaft and the output (vertical) screwed shaft, engaged via the worm-gear.

Barenten Suciu is with the Department of Intelligent Mechanical Engineering, Fukuoka Institute of Technology, Fukuoka, 811-0295 Japan (phone: +81-92-606-4348; fax: +81-92-606-0747; e-mail: suciu@fit.ac.jp).

Output shaft rotates together with the worm wheel, as well as the upper and lower sleeves, since an anti-rotation key is used to prevent the relative motion between them. Travelling nut translates upward/downward when the output shaft rotates clockwise/counter-clockwise. This allows the displacement of a certain loading force F past a certain stroke S (Figs. 2 and 3). Sliding contact between the screwed shaft and the travelling nut is lubricated through the grease nipple shown by Fig. 1.

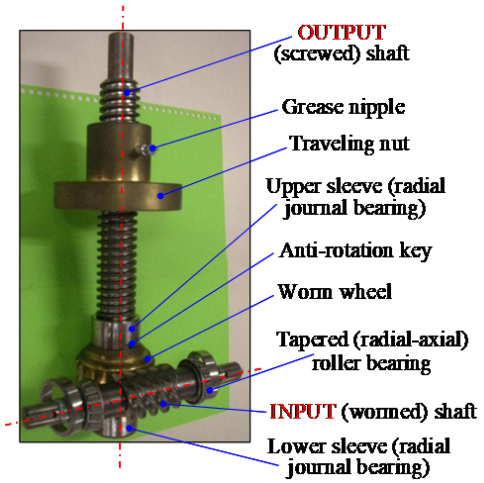

Fig. 1 Photograph of the input and output shafts of the designed SWGMT, engaged via the worm-gear

Output shaft is axially supported by two thrust ball bearings (Figs. 2 and 3), placed at the upper and lower ends of the worm wheel. Moreover, the output shaft is radially sustained by the upper and lower journal bearings. On the other hand, two tapered radial-axial roller bearings are holding the input shaft, which is driven by an electrical motor via a coupling (not shown) and an end key (Fig. 4). Thus, the SWGMT transmits the power from the electrical motor to the travelling nut, transforms the motor rotational movement into the translational motion of the nut, changes the power flow from horizontal to vertical direction, and reduces the motor higher rotational speed to lower rotational speed of the output screwed shaft. In this way, the desired relatively low translational speed of the travelling nut, i.e., of the loading force, can be achieved.

Screw-worm gear mechanism is accommodated by a case (Fig. 2), which is then closed and sealed at its upper, lower and lateral parts by three types of covers (see Figs. 3 and 4).

SWGMT can be assembled in such a way that the output shaft is loaded either by a compressive force (Fig. 2 (a)), or by a tensile force (Fig. 2 (b)). Since buckling of the output shaft

might occur under compressive loading, the design of the SWGMT will be conducted in this more dangerous case.

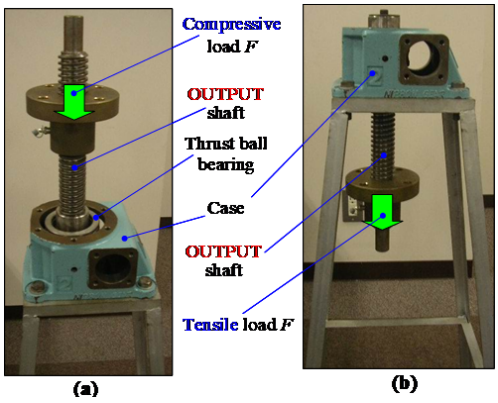

Fig. 2 (a) Compressive load, and (b) tensile load acting on the output shaft of the screw-worm gear mechanism, which, as shown in the above photographs, it is placed inside a case

III. Classical and 3D-Computer Aided Design Methods of the SWGMT

Classical design was performed according to the procedures described by [15], [17], and the tri-dimensional computer-aided design was carried out by using the SolidWorks software [18]. In order to confirm the adequate fitting of the various members of the SWGMT, the assembly module of the SolidWorks was employed. Then, the main parts were printed in ABS resin by using a Cube-type 3D-printer. After polishing the fitting surfaces of the components by using sandpaper, compatibility of the parts with their counter-parts and then the correct assembly of all the parts were verified. Thus, Fig. 3 illustrates a frontal bi-dimensional (2D) view of the designed SWGMT, showing the consisting parts, the compressive loading of the output screwed shaft, and some of the main geometrical parameters, such as the stroke S of the travelling nut, and the height H of the case. Additionally, Fig. 4 presents a top 2D-view of the designed SWGMT, illustrating the consisting parts, and some of the main geometrical parameters, such as the length L of the case, and the width B of the SWGMT, which coincides with the length of the input wormed shaft.

In order to evaluate the effectiveness of the design process, three performance parameters (total efficiency, specific load, and specific output work) of the SWGMT are defined. Firstly, the total efficiency η_t can be written as:

$$\eta_t = \eta_s \times \eta_w \times \eta_b \tag{1}$$

where η_s is the efficiency of the screwed part of the SWGMT, η_w is the efficiency of the worm-gear, and η_b is the overall efficiency of the bearings, including the radial journal bearings, the thrust ball bearings, and the tapered roller bearings.

Maximization of the total efficiency is desirable in order to achieve energy saving, and hence, environmental protection during the machine service life. Then, the specific load Σ_L can be defined as the ratio of the axial loading force F, supported by the output screwed shaft, and the volume of the box in which the case of the SWGMT can be circumscribed:

$$\Sigma_L = \frac{F}{L \times B \times H} \tag{2}$$

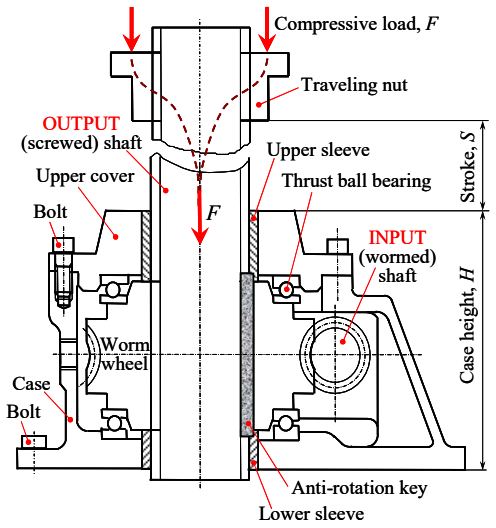

Fig. 3 Frontal 2D-view of the designed SWGMT, showing the consisting parts, the compressive loading of the output shaft, and some of the main geometrical parameters (the nut stroke and case height)

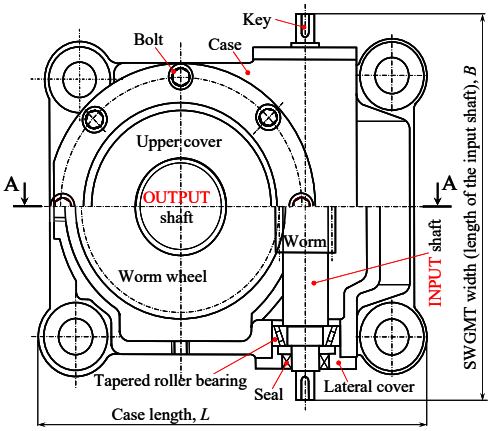

Fig. 4 Top 2D-view of the designed SWGMT, showing the consisting parts, and some of the main geometrical parameters, such as the case length and the width of the SWGMT

Compact design of the SWGMT is achieved when the box volume $L \times B \times H$ becomes minimal. However, from the strength analysis of the parts, one arrives to conclusion that their dimensions increase at the augmentation of the load F. Thus, the specific load Σ_L appears as a more suitable parameter of evaluation, which has to be maximized for efficient design. Moreover, since the stroke of travelling nut dictates the length of the output shaft, in order to include in the evaluation such effect, the so-called specific output work of the

SWGMT is defined as follows, and maximized during the design process:

$$\Sigma_W = \frac{F \times S}{L \times B \times H} \quad (3)$$

With the purpose of illustrating the computer aided design process, output screwed shaft is shown as a photo of the real shaft made in S45C steel (Fig. 5 (a)), as a 3D drawing obtained by using the SolidWorks (Fig. 5 (b)), and as a photo of the 3D printed shaft in ABS resin (Fig. 5 (c)). Design process includes not only the screw, but also the cylindrical shaft end, and the anti-rotation key groove. Printed trapezoidal screw requires to be carefully polished in order to achieve good engagement with its counter-parts, i.e. the travelling nut and the worm wheel.

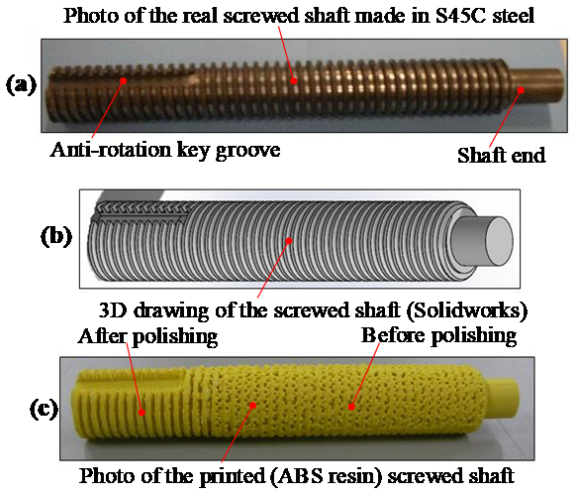

Fig. 5 (a) Photo of the real shaft, (b) 3D drawing of the output shaft, and (c) photo of the 3D printed shaft in ABS resin, illustrating the design process of the output screwed shaft

Fig. 6 illustrates a photo of the real travelling nut made in CAC502C bronze. Design process includes not only the inner trapezoidal screw, but also the screwed hole for the grease nipple, the inner groove for grease accumulation, and the flange with its bolt holes. Supplementary, Figs. 7 and 8 present the 3D drawing created with SolidWorks, and the printed travelling nut, respectively.

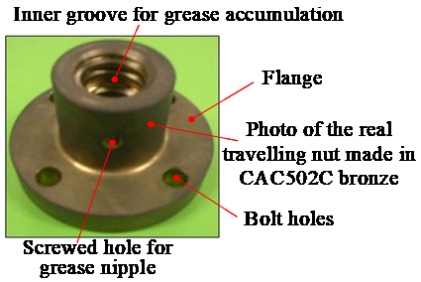

Fig. 6 Design process of the travelling nut, showing a photo of the real nut made in CAC502C bronze

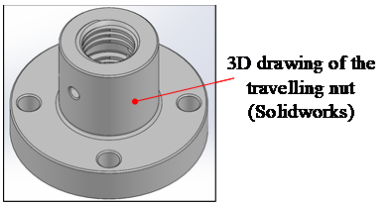

Fig. 7 Design process of the travelling nut, showing the 3D drawing obtained by using the SolidWorks software

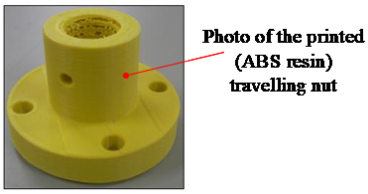

Fig. 8 Design process of the travelling nut, showing a photo of the printed nut in ABS resin

Fig. 9 illustrates a photo of the real worm wheel made in CAC502C bronze. Design process includes not only the external tooth, but also the inner trapezoidal screw and the inner groove for the insertion of the anti-rotation key. Additionally, Figs. 10 and 11 show the 3D drawing created with SolidWorks, and the printed worm wheel, respectively.

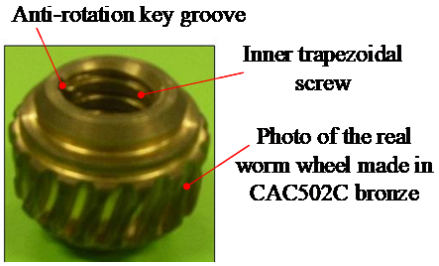

Fig. 9 Design process of the worm wheel, showing a photo of the real wheel made in CAC502C bronze

Since the output screwed shaft engages both the travelling nut and the worm wheel, the same trapezoidal screw is used, but it has different purposes. On one hand, the screw purpose is to transmit motion through the sliding contact between the output shaft and the nut, and, on the other hand, to assemble the worm wheel on the output shaft, via a fixed-type contact.

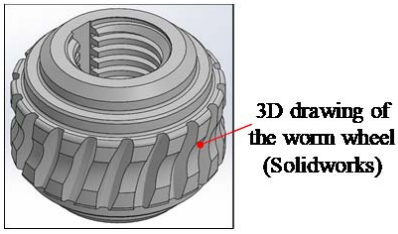

Fig. 10 Design process of the worm wheel, showing the 3D drawing obtained by using the SolidWorks software

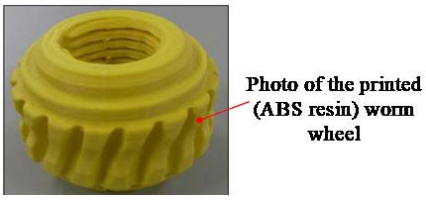

Fig. 11 Design process of the worm wheel, showing a photo of the printed wheel in ABS resin

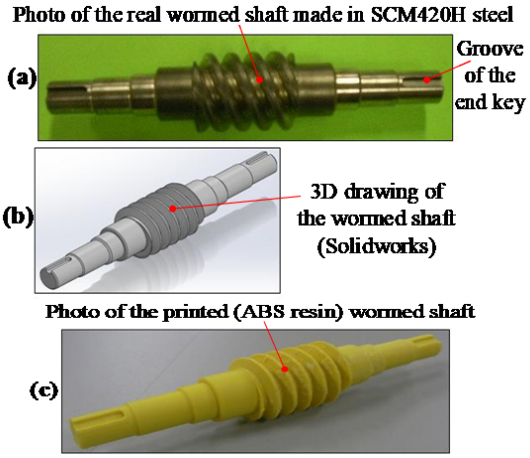

Fig. 12 (a) Photo of the real shaft, (b) 3D drawing of the input shaft, and (c) photo of the 3D printed shaft in ABS resin, illustrating the design process of the input wormed shaft

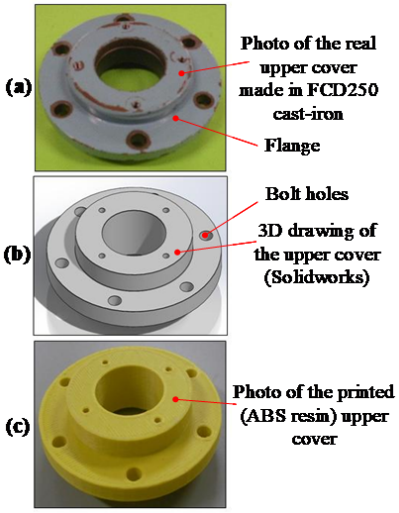

Fig. 13 (a) Photo of the real cover, (b) 3D drawing of the upper cover, and (c) photo of the 3D printed cover in ABS resin, illustrating the design process of the upper cover

Fig. 12 shows the input wormed shaft, as a photo of the real shaft made in SCM420H (Fig. 12 (a)), as a 3D drawing obtained with SolidWorks (Fig. 12 (b)), and as a photo of the 3D printed shaft in ABS resin (Fig. 12 (c)). Design process includes not only the worm helix, but also contact surfaces with the tapered roller bearings, and seals, as well as the groove of the end key.

Fig. 13 presents the upper cover of the case, as a photo of the real cover made in FCD250 cast-iron (Fig. 13 (a)), as a 3D drawing created with SolidWorks (Fig. 13 (b)), and as a photo of the 3D printed cover in ABS resin (Fig. 13 (c)). Design process mainly aims to properly decide the dimensions of the flange, and of the bolt holes.

Fig. 14 illustrates the lower cover of the case, as a photo of the real cover made in FCD250 cast-iron (Fig. 14 (a)), as a 3D drawing made with SolidWorks (Fig. 14 (b)), and as a photo of the 3D printed cover in ABS resin (Fig. 14 (c)). Again, the design process mainly intends to properly decide all the dimensions of the flange, and of the bolt holes.

Fig. 15 shows the lateral cover of the case, as a photo of the real cover made in FCD250 cast-iron (Fig. 15 (a)), as a 3D drawing obtained with SolidWorks (Fig. 15 (b)), and as a photo of the 3D printed cover in ABS resin (Fig. 15 (a)). During the design process, one chiefly decides the suitable accommodation of the seals, and the dimensions of the bolt holes.

In the end of this section, Figs. 16-18 illustrate the casing assembly of the designed transmission, consisted of the actual case which is provided with the upper, lower and lateral covers. Concretely, Fig. 16 shows a photo of the real assembly, in which the case is made in FCD250 cast-iron, Fig. 17 illustrates the 3D drawing assembled in SolidWorks, and Fig. 18 presents the printed assembly in ABS resin.

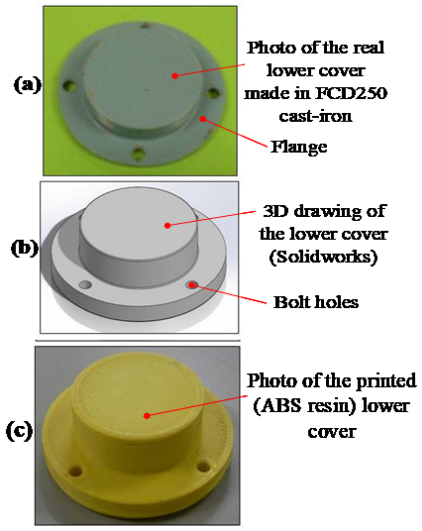

Fig. 14 (a) Photo of the real cover, (b) 3D drawing of the lower cover, and (c) photo of the 3D printed cover in ABS resin, showing the design process of the lower cover

Based on Figs. 16-18 of the casing assembly, one proves the geometrical compatibility of the parts with their counter-parts, obtained through both the classical, and computer aided design procedures.

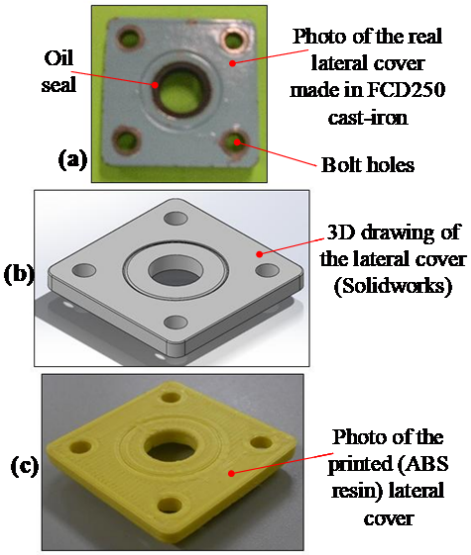

Fig. 15 (a) Photo of the real cover, (b) 3D drawing of the lateral cover, and (c) photo of the 3D printed cover in ABS resin, illustrating the design process of the lateral cover

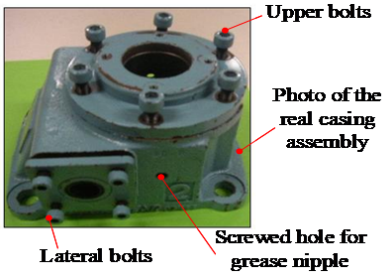

Fig. 16 Photo of the real casing assembly, consisted of the actual case, and three types of covers, which are fixed with bolts on the case

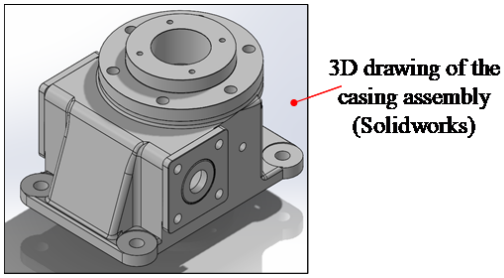

Fig. 17 Assembly drawing of the casing, where the components are assembled in SolidWorks

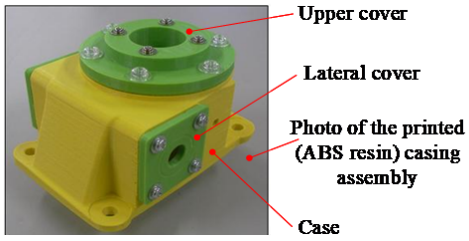

Fig. 18 Casing assembly printed in ABS resin

IV. Results and Discussions

Figs. 19 and 20 illustrate the variation of the SWGMT total efficiency versus the travelling velocity V of the nut. Figs. 21 and 22 show the variation of the SWGMT specific load Σ_L against the travelling velocity V of the nut. Figs. 23 and 24 present the variation of the SWGMT specific output work Σ_W versus the travelling velocity V of the nut. Results illustrated in Figs. 19-24 are obtained for various values of the stroke of the travelling nut, i.e., $S = 0.1$, 0.5, 0.9, 1.3, and 1.7 m. Figs. 19, 21, and 23 present the calculations for a relatively lower loading force of $F = 50$ kN. Figs. 20, 22, and 24 show the results for a relatively higher loading force of $F = 400$ kN.

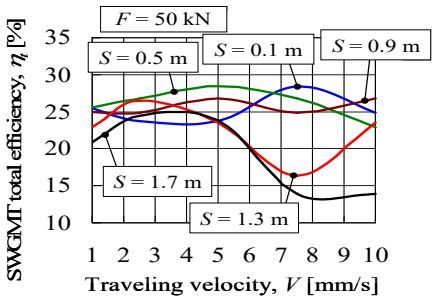

Fig. 19 Variation of the SWGMT total efficiency versus the travelling velocity of the nut, corresponding to various strokes of the nut, and obtained for a relatively lower loading force of 50 kN

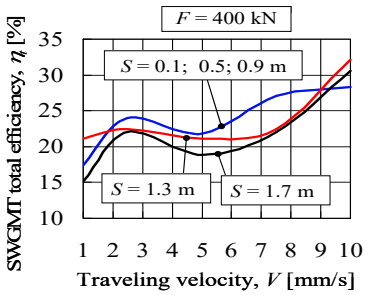

Fig. 20 Variation of the SWGMT total efficiency versus the travelling velocity of the nut, corresponding to various strokes of the nut, and obtained for a relatively higher loading force of 400 kN

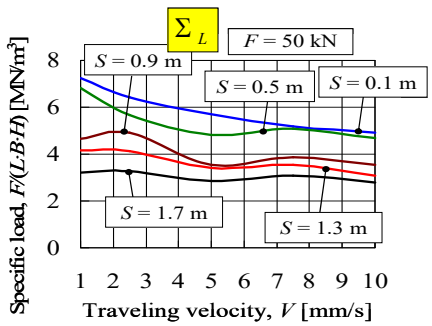

Fig. 21 Variation of the SWGMT specific load versus the travelling velocity of the nut, corresponding to various strokes of the nut, and obtained for a relatively lower loading force of 50 kN

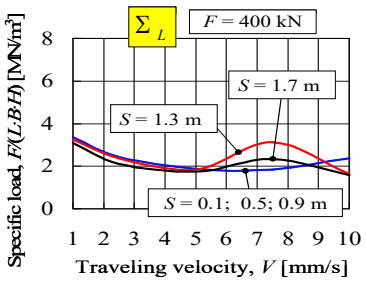

Fig. 22 Variation of the SWGMT specific load versus the travelling velocity of the nut, corresponding to various strokes of the nut, and obtained for a relatively lower loading force of 400 kN

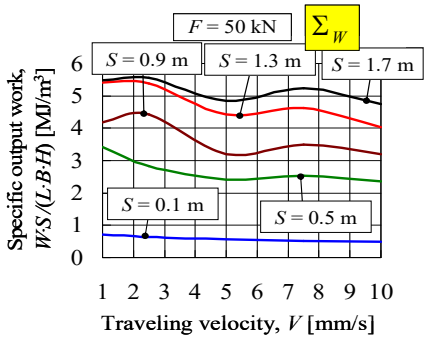

Fig. 23 Variation of the SWGMT specific output work versus the travelling velocity of the nut, corresponding to various strokes of the nut, and obtained for a relatively lower loading force of 50 kN

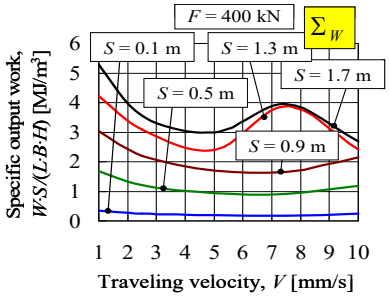

Fig. 24 Variation of the SWGMT specific output work versus the travelling velocity of the nut, corresponding to various strokes of the nut, and obtained for a relatively lower loading force of 400 kN

From Figs. 19 and 20, one observes that the total efficiency of the SWGMT has quite a complex dependence on the velocity and stroke of the travelling nut. However, as general tendency, the total efficiency appears as relatively higher for shorter strokes, and, relatively lower for longer strokes.

For the higher loading force of $F = 400$ kN, and for the shorter strokes of $S = 0.1, 0.5, 0.9$ m, the influence of stroke on the total efficiency fades (see Fig. 20). For this reason, the total efficiency, as a standalone parameter, cannot be satisfactorily used to evaluate the effectiveness of the design process.

For $F = 400$ kN, although the efficiency exceeds 30% in the range of high velocities and strokes of the travelling nut (see Fig. 20), the total efficiency of the SWGMT occurs as relatively poor. However, by replacing the trapezoidal screw with a ball-screw, i.e. by replacing the sliding friction with rolling friction, the total efficiency of SWGMT can be considerably augmented.

For lower loading force ($F = 50$ kN, see Fig. 21), as general tendency, the specific load decreases at augmentation of the stroke and velocity of the traveling nut. However, for higher loading force ($F = 400$ kN, see Fig. 22), the dependence of specific load against stroke cannot be clearly identified. Again, similar to the total efficiency, the specific load, as a standalone parameter, cannot be satisfactorily employed to determine the quality of the design process. On the other hand, the dependence of the specific output work can be clearly identified versus the velocity and stroke of the travelling nut, regardless the magnitude of the loading force (see Figs. 23 and 24). For example, the specific output work decidedly increases against the stroke. Consequently, the specific output work appears as a more suitable parameter in the quest of evaluating the effectiveness of the design process.

V. Conclusions

In this work, the common and computer aided techniques were employed to design a screw-worm gear mechanical transmission, and the effectiveness of the design process was assessed based on the total efficiency, the specific load, and the specific output work. Main conclusions can be summarized as:

1) Total efficiency of the mechanical transmission occurs as relatively poor, but it can be augmented by replacing the trapezoidal screw with a ball-screw;
2) Excellent compatibility was obtained between parts and their counter-parts, by using the assembly module of the SolidWorks software. However, contact surfaces should be carefully polished after 3D-printing in order to achieve the appropriate engagement conditions between the parts and their counter-parts;
3) Instead of choosing the total efficiency or the specific load, one might employ the specific output work, to decidedly estimate the quality of the design process.

Acknowledgment

Support during the 3D computer aided design and printing of the screw-worm gear mechanical transmission, from the part of Mr. H. Nakamura, former student at the Department of Intelligent Mechanical Engineering, Fukuoka Institute of Technology, is acknowledged.

References

[1] J. A. Collins, H. R. Busby, and G. H. Staab, *Mechanical Design of Machine Elements and Machines*. New York: John Wiley and Sons, 2009, pp. 231–890.
[2] M. Izawa, *Machine Design Engineering*. Tokyo: Rikogakusha, 2010, pp. 1–342 (in Japanese).
[3] R. C. Johnson, *Optimum Design of Mechanical Elements*. New York: John Wiley and Sons, 1961, pp. 1–301.
[4] R. C. Juvinall, and K. M. Marshek, *Fundamentals of Machine Component Design*. New York: John Willey and Sons, 2006, pp. 1–769.
[5] R. L. Mott, *Machine Elements in Mechanical Design*. New Jersey: Prentice-Hall, 2004, pp. 11–872.
[6] H. A. Rothbart, *Mechanical Design and Systems Handbook*. New York: McGraw-Hill, 1985, pp. 7–173.

[7] M. F. Spotts, T. E. Shoup, and L. E. Hornberger, *Design of Machine Elements*. New Jersey: Prentice-Hall, 2003, pp. 23–324.
[8] G. W. Stachowiak, and A. W. Batchelor, *Engineering Tribology*. Amsterdam: Elsevier, 2005, pp. 1–795.
[9] T. Tsukada, Y. Yoshimura, S. Kurosaki, and F. Yagishita, *Methodology of Machine Design*. Tokyo: Morikita, 2015, pp. 1–211 (in Japanese).
[10] J. Angeles, and E. Zakhariev, *Computational Methods in Mechanical Systems: Mechanism Analysis, Synthesis, and Optimization*. Berlin: Springer, 1998, pp. 1–425.
[11] F. De Bona, and G. Jacazio, "Simulation of Mechanical Drives with Generalized Power Losses," *Mathematical and Computer Modelling*, 11, pp. 1178–1182, 1988.
[12] A. A. Oledzki, "Modeling and Simulation of Self-locking Drives," *Mechanism and Machine Theory*, 30(6), pp. 929–942, 1995.
[13] E. Polak, *Computational Methods in Optimization: A Unified Approach*. New York: Academic Press, 1971, pp. 1–329.
[14] D. J. Wilde, *Global Optimum Design*. New York: John Wiley and Sons, 1978, pp. 5–67.
[15] C. V. Suciu, H. Goto, and H. Abiru, "Modeling and Simulation of a Screw-Worm Gear Mechanical Transmission to Achieve its Optimal Design under Imposed Constraints," *Journal of Algorithms and Computational Technology*, 5(2), pp. 363–382, 2011.
[16] P. Gallina, "Vibration in Screw Jack Mechanisms Experimental Results," *Journal of Sound and Vibration*, 282(3-5), pp. 1025–1041, 2005.
[17] K. Sano, *Design of the Screw Jack*. Tokyo: Power Publisher House, 1994, pp. 1–156 (in Japanese).
[18] G. Onwubolu, *Computer-Aided Engineering Design with SolidWorks*. London: Imperial College Press, 2013, pp. 1–721.

Barenten Suciu was born on July 9, 1967. He received Dr. Eng. Degrees in the field of Mech. Eng. from the Polytechnic University of Bucharest, in 1997, and from the Kobe University, in 2003. He is working as Professor at the Department of Intelligent Mech. Eng., Fukuoka Institute of Technology. He is also entrusted with the function of Director of the Electronics Research Institute, affiliated to the Fukuoka Institute of Technology. He is member of JSME, JSAE, and JSASS. His major field of study is the tribological and dynamical design of various machine elements.